공학석사학위논문

미세 물체 수송을 위한
니티놀 마이크로 로봇

Ni-Ti Micro Robot for Fine-object Transportation

2021년 8월

서울대학교 대학원
기계공학부

김 대 현

미세 물체 수송을 위한
니티놀 마이크로 로봇

Ni-Ti Micro Robot for Fine-object Transportation

지도교수 안 성 훈

이 논문을 공학석사 학위논문으로 제출함

2021 년 4 월

서울대학교 대학원
기계공학부
김 대 현

김 대 현 의 공학석사 학위논문을 인준함

2021 년 6 월

위 원 장 : 차 석 원

부위원장 : 안 성 훈

위 원 : 이 호 원

Abstract

A micro-robot is an attractive tool that performs micro-scale tasks within the system by remote control. Most micro-robots are driven by an external force and its characteristic differs according to the type of the external force. Therefore, micro-robots have been developed to utilize the type of external force suitable for their respective application fields. Among various external forces, a light-driven micro-robot has superior controllability in terms of precision and regionality. Recently, lots of studies have been conducted on micro-robot for performing micro-scale tasks in bio-medical fields such as drug transport, surgery and diagnosis.

Especially in micro-object transportation, since sophisticated control is required, a light-driven micro-robot which has excellent controllability is advantageous. Micro-robots for transportation so far have focused on force, speed and control, but a few of them have a function of holding objects to avoid object loss.

Our micro-object transportation Ni-Ti structure robot(MTNs) not only has sufficient thrust force and speed but also has the capability of holding objects and physically separating them from external systems, thus demonstrating the advantage of excellent transport stability and controllability. It can be fabricated and controlled automatically by a vision-guided laser control system. In consideration of mass production, we designed the micro-robot so that the fabrication process has low cost in terms of time, price and labor, and can be operated by commercial equipment. The newly designed transport

micro-robot, which displays holding capability and enhanced control, can be used as an actuator in lab-on-a-chip testing.

Keywords : Micro-robot, Micro transportation, Laser driven, Formation morphing control, Micro manipulation, Shape memory alloy

Student Number : 2019-24859

Table of Contents

List of Figures

List of tables

Chapter 1. Introduction

1.1. Reviews on micro robots for bio-medical application

A micro-robot is an attractive tool that performs micro-scale tasks within the system by remote control. The advantage of remote control is that it is likely to minimize the side effects on the surrounding areas because it operates within the system, unlike other wired manner methods that require penetration between systems. This advantage has contributed to various research of micro-robot for bio-medical applications such as drug delivery, surgery and sensing. The enteric micromotor[28] is developed for precise delivery of therapeutic payloads to targeted disease sites. By tuning the thickness of pH-sensitive layer, it can selectively activate motor. The microneedle[29] which is consist of CoNi tube and stainless steel needle is for a surgery in many hard-to-reach locations in human body. it is controlled by magnetic in a wireless way. The bio-receptors[30] with artificial nanomoters can detect and isolate biological targets such as proteins, nucleic acids and cancer cell

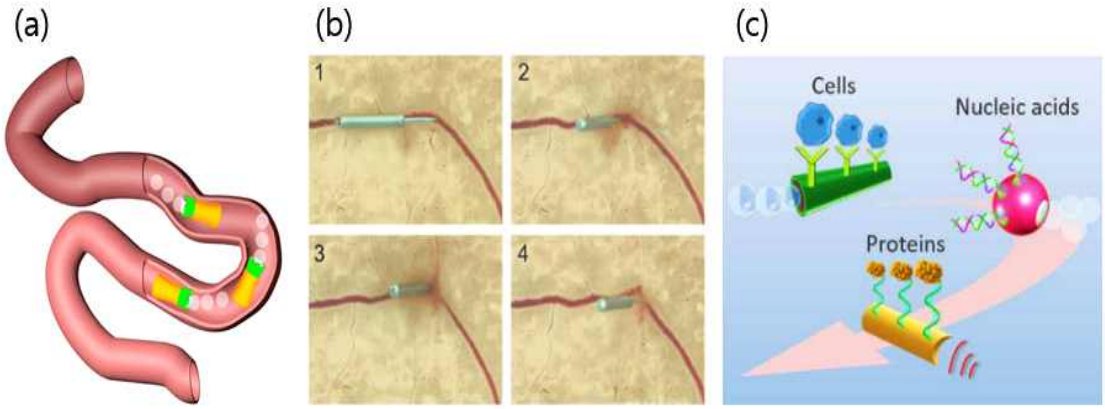

Figure 1. Micro robots for bio-medical application. a) the entric micro motor[28], b) the micro needle[29], c) the bio-receptor[30]

1.2. Reviews on micro transportation

The magnetic swarm micro-robot [3] can transport micro-objects of various sizes through locomotion by swarm control, However, it has a flaw in which the target object cannot be fully grasped, which can lead to object loss. On the other hand, the helical micro-robot [4] was developed such that it completely holds the target object by putting the object inside the body and sealing it with the cap on the front body. However, this is difficult to control and has a limitation in that the size of the object is fixed. The large number of studies including optical tweezers [5] which hold and move objects using a laser and micro-gripper robot[6] gripping through micro patterns, clearly indicate that there is a demand for a holding function in transporting micro objects.

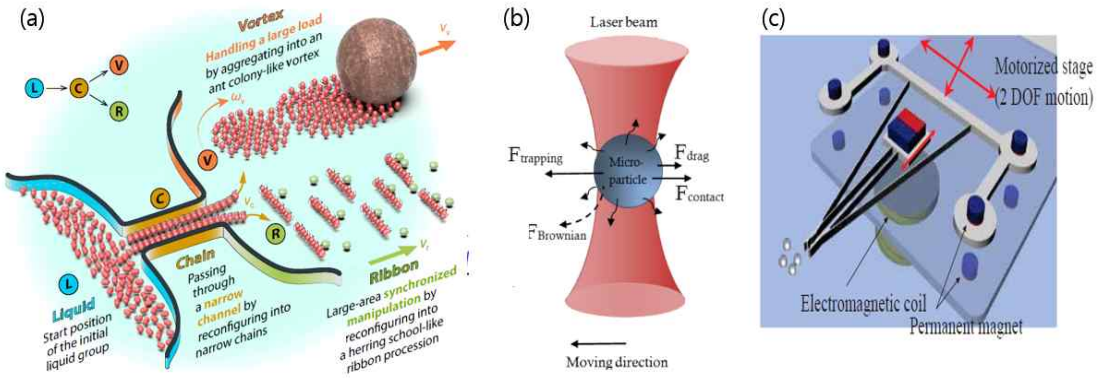

Figure 2. Micro transportation tools. a) the magnetic swarm robot[3], b) the optical tweezer[5], c) the micro-gripper robot[6]

1.3. Reviews on micro robots using external forces

Most micro-robots use an external force for power supply and user-defined control (active control), As the driving characteristic differs depending on the type of external force, it is important to select the specific type of external force according to the application. Micro-robots developed for in-vivo applications are controlled by biochemicals[31] or magnetic fields[3,4,6,15] that can penetrate the human body. Meanwhile, micro-robot for in-vitro application (on-chip) usually use acoustic[33] or light[1,2,11] as an external force for high speed and regional fine control. In particular, a light-driven micro-robot can be controlled very finely, so it is suitable for use in transporting application

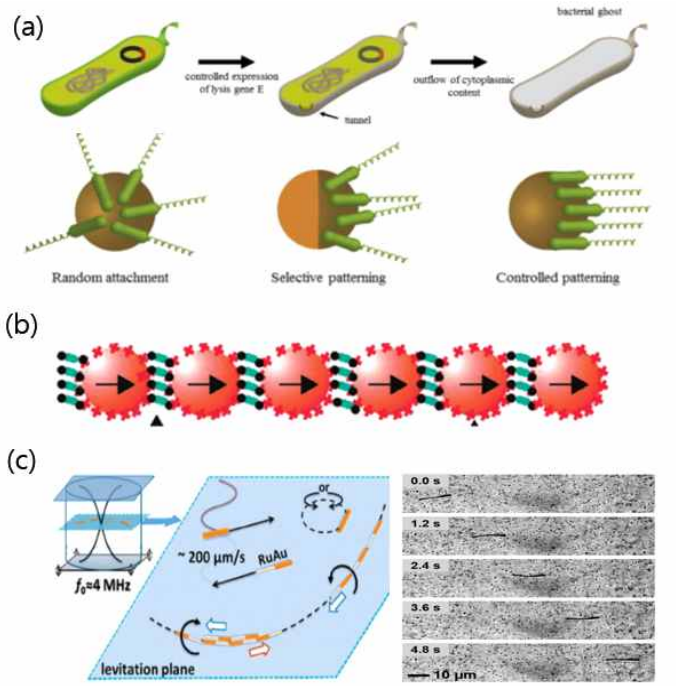

Figure 3. External forces for micro robot driving. a) biochemical[31], b) magnetic [32], c) acoustic[33]

1.4. Reviews on light-driven Ni-Ti micro robots

Recently, Ni-Ti micro-robots have been developed exploiting the principle of heat generation due to the difference in laser absorption rate in the UV wavelength band of water and Ni-Ti. The Kirigami pattern Ni-Ti micro-robot [2] generates a thermal gradient to gain propulsion momentum. This robot which following the laser displays easy and precise control. However, it shows a limitation in terms of productivity since micro-patterning via micro fabrication equipment such as focused-ion-beam (FIB) is time-consuming and expensive. In order to improve productivity, the simple Ni-Ti micro-robot [1] was designed to simplify the fabrication process, while showing benefits in terms of speed and controllability. The robot is powered by bubble expansion resulting from local heating by the laser which evaporates the medium.

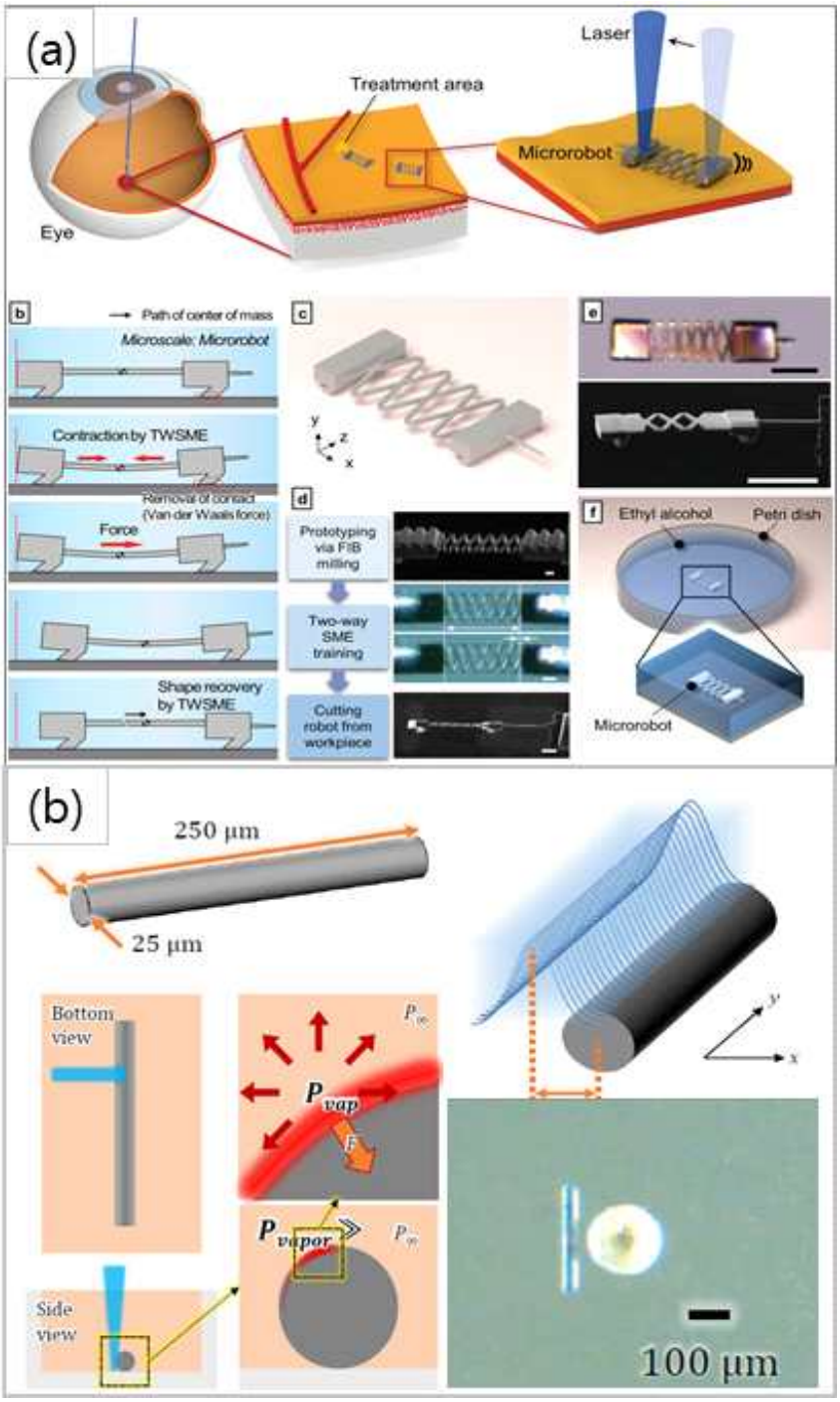

Figure 4. Ni-Ti micro robots. a) Kirigami pattern Ni-Ti micro robot [2], b) Ni-Ti unit [1]

1.5. Purpose of Research

In this study, we have demonstrated that the proposed micro-object transporting Ni-Ti structure (MTNs) has enhanced controllability, energy efficiency and holding capability. Fig 1. shows the schematic of the fabrication process of the MTNs. The robot is designed with an emphasis on productivity to be suitable for mass production. The fabrication process consists of commercial equipment for accessibility and low price. We constructed the vision-guided laser control system to automate the fabrication process and lower the labor cost. Based on the force measurement results, we compared energy efficiency of MTNs with other light-driven micro-robots. The transporting experiment was conducted to show the functionality of MTNs.

Chapter 2. Ni-Ti unit

2.1. Actuation mechanism

According to a previous study [1] that developed the Ni-Ti unit, the unit is operated by the expansion force of bubbles generated by laser local heating. When a unit immersed in a medium such as water or ethanol is irradiated with a laser in the UV wavelength band, the Ni-Ti surface is locally heated by the difference in laser absorption between the medium and Ni-Ti. Then, the surrounding medium is instantaneously vaporized in the local heating area, resulting in explosive volume expansion. The bubble generated by the above process pushes the unit, thereby gaining momentum and moving forward.

In the previous study [1], the hypothesis was established by proving that the unit speed calculated by considering the fluid resistance and the surface friction force and the value obtained through the actual experiment are similar. The speed of the unit is 80 mm/s at a laser intensity of 30 mW/mm^2. Considering that the body is 250 μm, it can be said that it moves at a speed of 320 times that of the body.

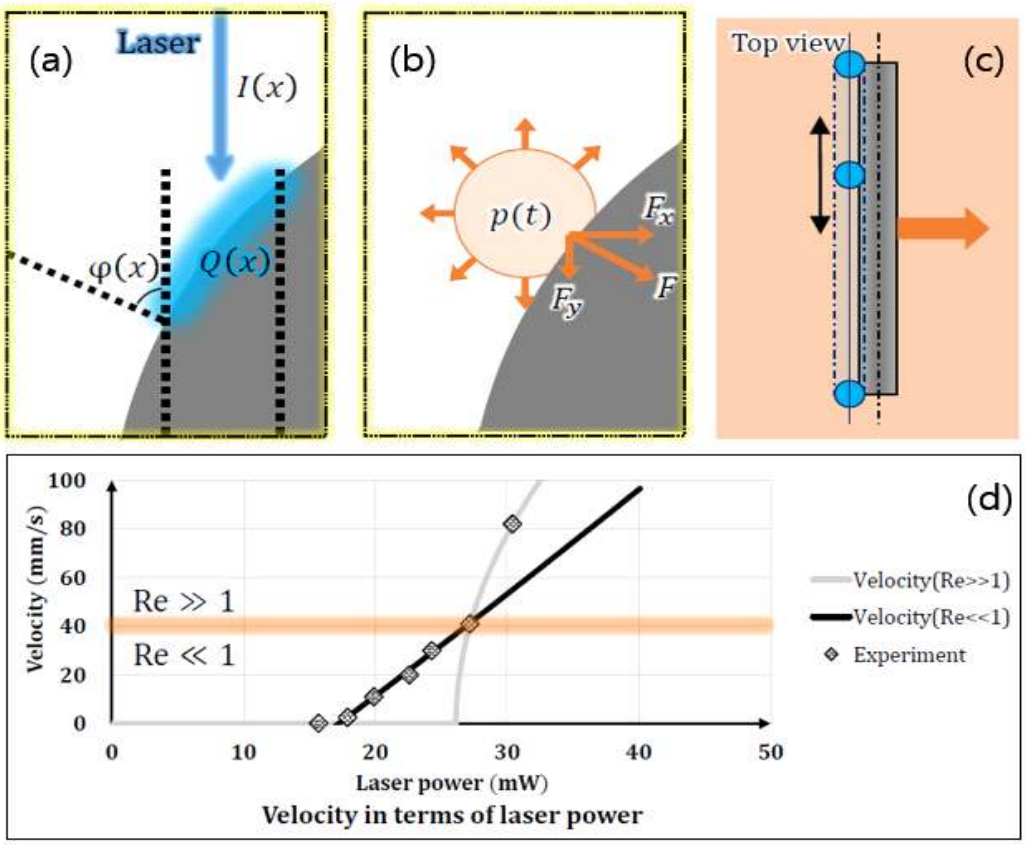

Figure 5. Actuation mechanism of Ni-Ti unit[1]. a) regional laser absorption, b) bubble expansion, c) top view when laser control, d) Comparison graph of theoretical speed and experimental value calculated based on the proposed hypothesis

2.2. Fabrication of Ni-Ti unit

The Ni-Ti unit used in this study was fabricated by cutting Ni-Ti wire of diameter using a cutter with distance between the blades. Exerting a force over the cutter placed vertically above the Ni-Ti wire resulted in an average yield of 30 element micro-robots. Then, by annealing them at 80° C for 45 minutes, the units were straightened out via the shape memory effect. Since the straightness of the unit is closely related to the stability of laser control, it is very important to straighten it through the annealing process. The ready units were cylindrical shape of 50 μm diameter and 300 μm length

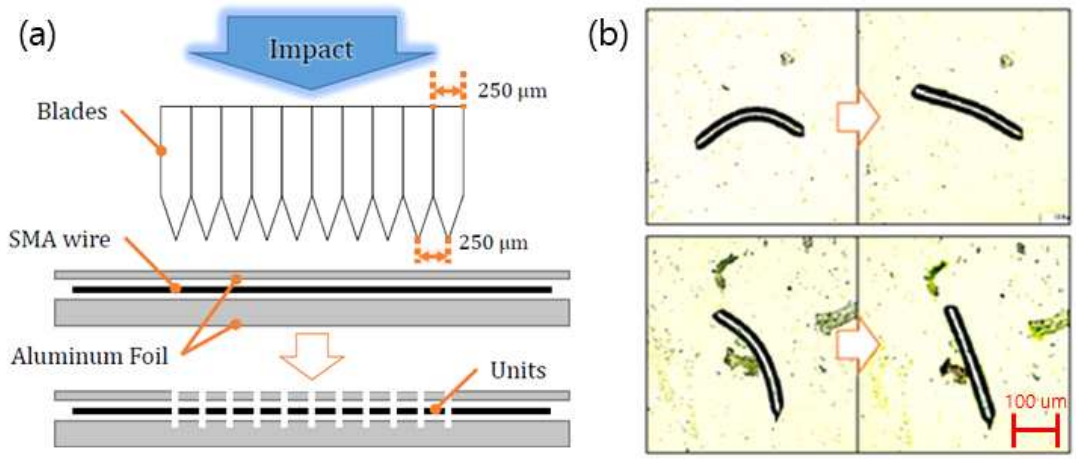

Figure 6. Fabrication process of Ni-Ti unit. a) chopping Ni-Ti wire using a cutter with distance between the blades, b) annealing process

Chapter 3. Fabrication process

3.1. Overview of fabrication process

We designed the MTNs to be fabricated at a low cost in terms of time, price and labor in consideration of mass production. The fabrication process equipment includes a cutter, laser, CCD camera and micro fluidic jetting equipment, all of which are used commercially.

Ni-Ti was selected as the material due to its characteristic resilience against plastic deformation caused by impact in the cutting process. Since the bent unit moves unpredictably, high production yield can be obtained using the material that can ensure the quality of straightness. Ni-Ti is also a biocompatible material that can be utilized for bio applications.

We set the shape of MTNs to a hexagon, showing that complex shapes can be formed by our automatic fabrication system. The structural shape varies depending on the size of the target object. We can choose the mode of MTNs according to the purpose of transportation. Fig 7. shows the two kinds of modes of MTNs. The open mode is reusable, so it can be used for transporting several objects quickly. The closed mode, which can secure the object, is for stable transportation. It can be expanded into cell form which can perform the storage/transport functions of a large number of micro objects by continuously adding same shape structures.

Fig 8. shows the whole fabrication process of MTNs. We will

explain all these processes one by one detail in this chapter.

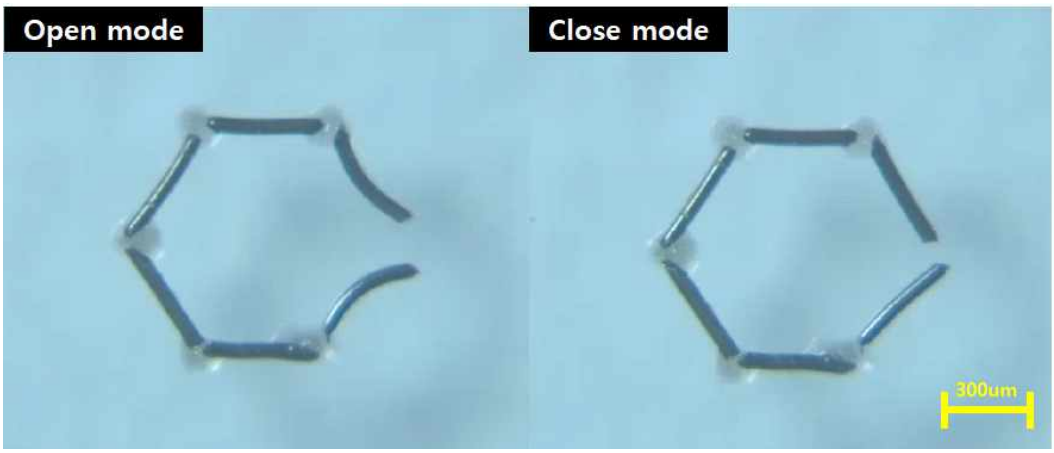

Figure 7. Mode conversion of MTNs through heating

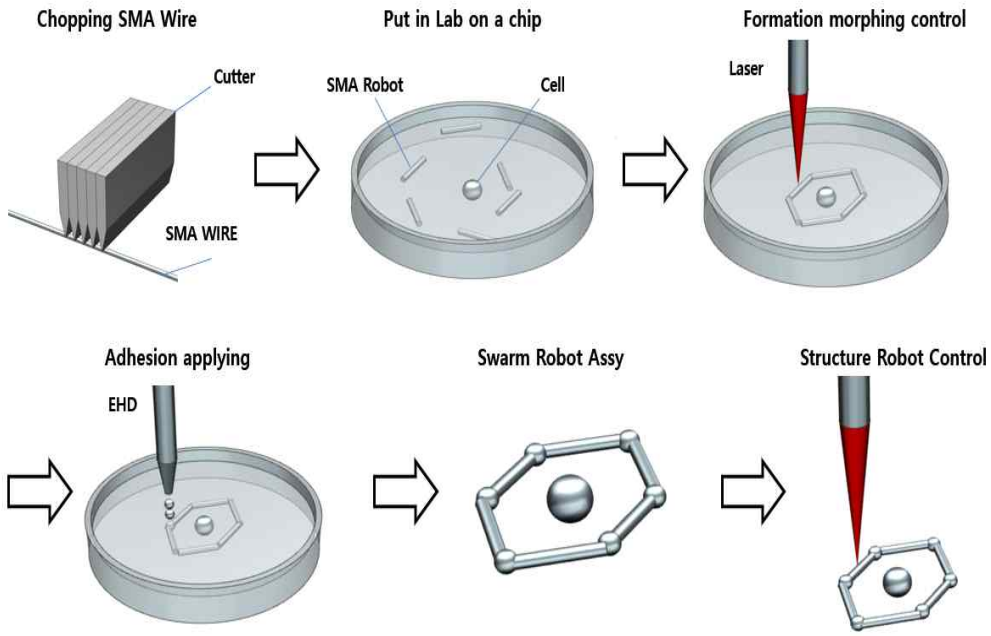

Figure 8. The fabrication process of MTNs

3.2. Formation morphing control

3.2.1. Single unit control

The Ni-Ti units manipulations occurred on a 4x3" glass slide covered with AF coating. First, a needle was used to insert 2 mL of saline solution on the glass slide. Then, the required number of the Ni-Ti units were placed into the solution, on the surface of the slide.

The Galvano laser scanner we used can irradiate the laser in a desired pattern by controlling the laser at high speed. The dot-shape control method is unstable cause it is very sensitive to the error of positional value which frequently occurs in the process of converting the pixel coordinate system of the camera to the laser coordinate system and the image processing. line pattern control method provides fast speed but needs a condition that the orientation of the unit should be parallel to the laser scan direction. The array pattern laser control method is robust to the position error of the unit and is convenient to control because it only needs to scan in the direction of proceeding regardless of the robot's orientation. After the array pattern laser scan, the final orientation of the unit is arranged perpendicular to the laser direction.

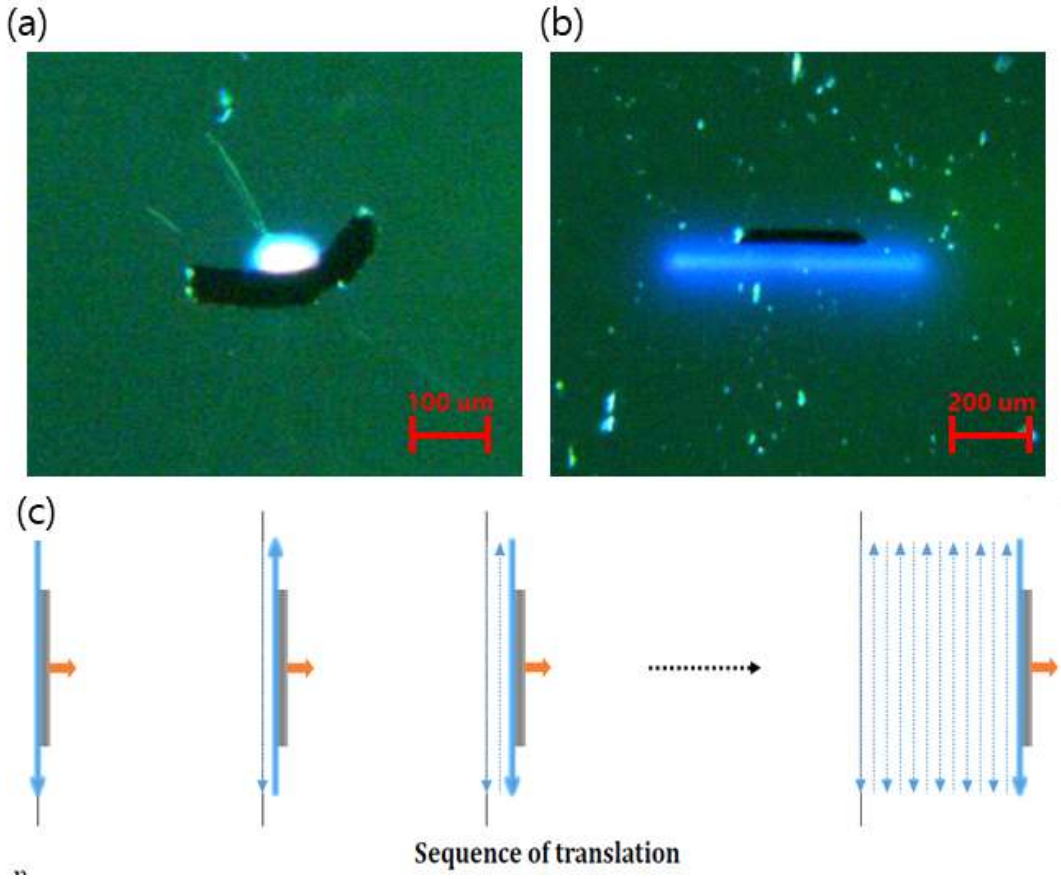

Figure 9. Single unit control[1]. a) Dot-shape laser control, b) Line-pattern laser control, c) Array-pattern laser control.

3.2.2. Vision-guided laser control system

We constructed the vision-guided laser control system that can arrange multiple Ni-Ti units to form a certain structure. The system is consist of CCD camera, the image processor, the path planner and the *Galvano* laser controller.

The high speed CCD camera *(Basler AG, Germany)*, which was connected to an *Olympus* lens microscope of ×100 magnification was positioned under the workspace. The resolution of each image frame obtained via the CCD camera was set to 1920×1080 pixels.

The images that capture the workspace in realtime are tossed to the image processor. The image processor detects the units in the workspace and extracts the position and orientation of the units using the canny edge detection function in the *OpenCV* library. The position of units is sent to the path planner which allocates units to the goal positions using the *Hungarian algorithm*[26], one of the combinatorial optimization algorithms that solve the assignment problem in polynomial time and which anticipated later primal dual methods. The allocation is updated at regular intervals so that it can flexibly respond to unexpected movement and external interference. The image processor and path planner were coded in Python programming language.

The *Galvano* laser controller operates following the path generated by the path planner. It is operated using *EZCAD* and positioned vertically above the glass slide.

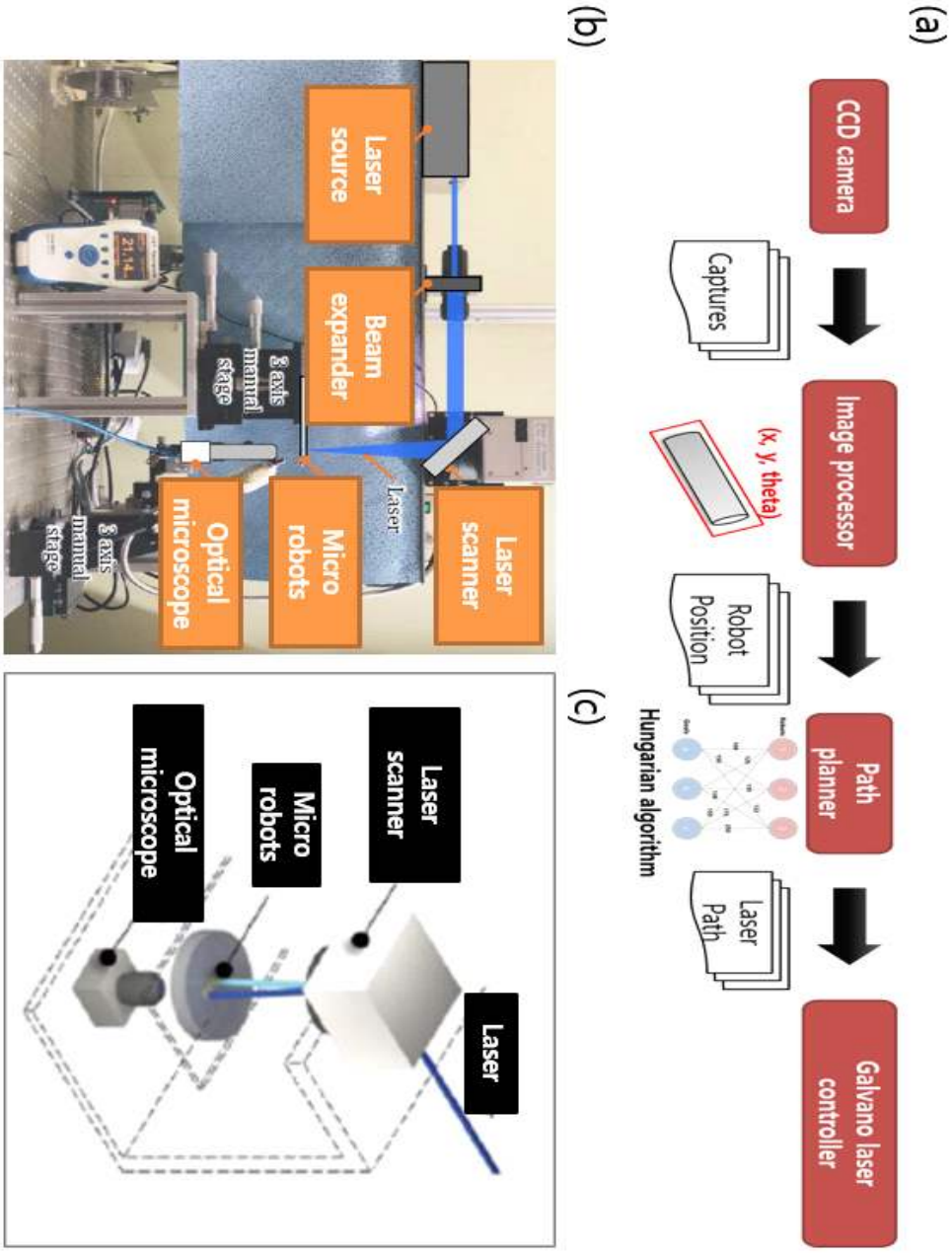

Figure 10. Vision-guided laser control system. a) flowchart of the control system, b,c) physical appearance of the control system

3.2.3. Control strategy

To form a certain structure with multiple Ni-Ti units at arbitrary initial positions, the orientation of the unit can be controlled as well as its position, but it has been mentioned earlier that the final orientation of the unit is perpendicular to the proceeding direction of the laser in the array-patter laser control method. Controlling the position of the unit is a simple task that can be performed by setting the laser proceeding direction as a straight line connecting the current position and the destination, whereas controlling the orientation of the unit requires complex path planning algorithms. However, we can deal with this task by a simple trick that breaks path planning down into two steps. Regardless of which path the robot has followed, the final orientation of the robot is determined by the direction of the last laser scan. Therefore, the focus should be on position control before the last laser scan. We set the intermediate target point outward in a direction perpendicular to each side from the final target point. The last laser scan can then be fixed and the robot's final position and orientation can be controlled as desired. The demonstration of this experiment is shown in Fig 11.

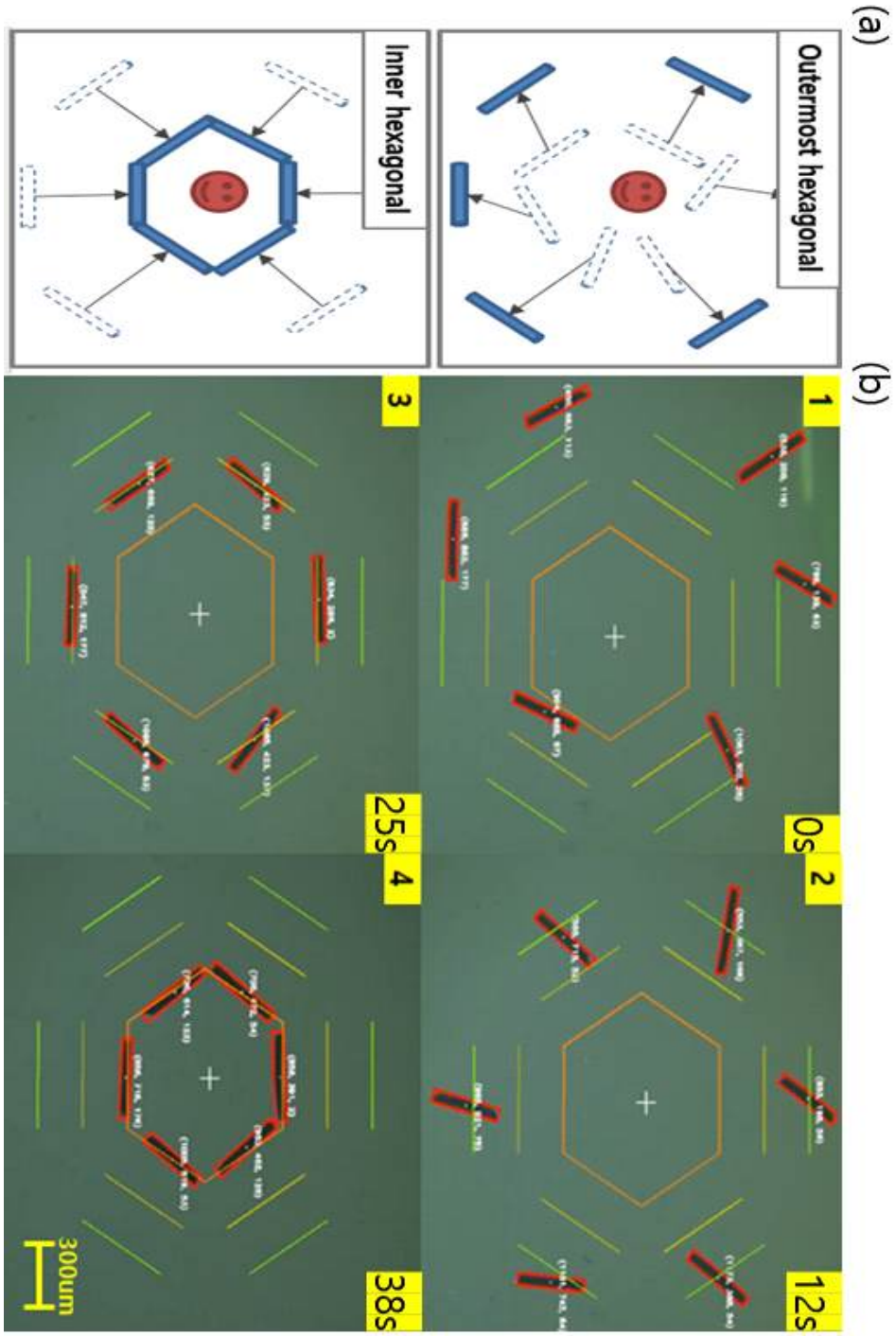

Figure 11. Formation morphing control. a) control strategy, b) demonstration of formation morphing control using the vision-guided control system

3.3. Bonding Process

3.3.1. Adhesion applying using EHD

An EHD(ElectroHydroDynamic) micro jet printer manufactured by *Enjet* was utilized to bond Ni-Ti units. The equipment applies a viscous fluid to a fine size by generating an electric field between the nozzle and metal adherent.

The fact that the EHD utilizes electric force near metal causes an issue in selecting the adhesive. In the case of using a low viscosity adhesive, it was impossible to laminate because the adhesive was attracted to the metal adherent with high surface energy due to the wetting property of the adhesive. Using high viscosity adhesives requires a high strength electrical force, so the nozzle height must be set low. In this case, the attractive force between the nozzle and the adherent causes the adherent to stick to the nozzle. Several tests were conducted to find a suitable adhesive that can be applied at minimum applying height ($=50\mu m$, same as robot height) and has low wetting property. Table 1. is the list of candidate adhesives, among them, we adopted the light curable adhesive, *Loctite AA3936* manufactured by *Henkel* with a cps of 8000. This is because the light curable adhesive cures quickly and can be cured immediately without changing the workspace.

The adhesive was laminated 3 times, about 20 μm each, to a final height of 60 μm. The adhesive was cured by irradiating an UV lamp for 30 s between each application. Fig 12. shows the MTNs of the final completion finished up to the bonding process.

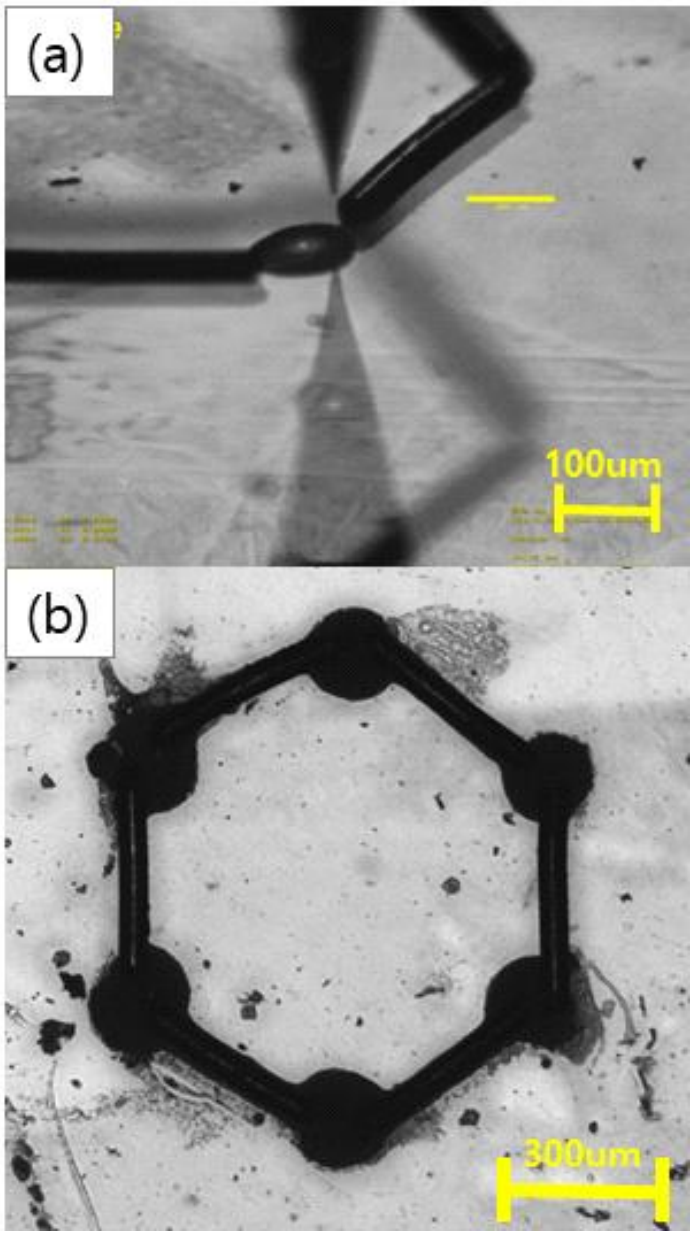

Figure 12. Adhesion applying by EHD. a) jetting adhesive on a joint position using EHD, b) the MTNs of the final completion up to the EHD adhesive applying

No.	Maker	Name	Property			
			Viscous(cps)	Curing time(min)	Curing method	Water soluble
1	Fuller	FH8621L	6500	10 at 80℃	Thermal	-
2	Henkel	AA3936	8000	1 at 500mW	UV	Insoluble
3	Fuller	FH8622S	10000	10 at 80℃	Thermal	-
4	Fuller	FH8632M	10000	30 at 80℃	Thermal	-
5	Three Bond	2086M	10000	30	Natural	-
6	Three Bond	2210	10000	30 at 90℃	Thermal	-
7	Henkel	Loctite 190024	10500	1 at 500mW	UV	Insoluble
8	Fuller	FH8626	12000	5 at 80℃	Thermal	-
9	Fuller	FH8623M	12500	5 at 80℃	Thermal	Soluble
10	Fuller	FH8634M	13000	5 at 80℃	Thermal	-
11	Henkel	Loctite 190024 lv	14000	1 at 500mW	UV	Insoluble
12	Fuller	FH8633	16500	5 at 80℃	Thermal	Soluble
13	Fuller	FH8633T	18000	1 at 500mW	UV	Insoluble
14	Fuller	FH8627M	20000	10 at 80℃	Thermal	-
15	Fuller	FH8634	22000	5 at 80℃	Thermal	-
16	Fuller	FH8632	25000	30 at 80℃	Thermal	-
17	Fuller	FH8636	25000	10 at 80℃	Thermal	-
18	Fuller	FH8633T	25000	5 at 80℃	Thermal	Soluble
19	Fuller	FH8516	30000	150	Natural	-
20	Fuller	FH8620	35000	20 at 80℃	Thermal	-
21	Fuller	EU1005	35000	10 at 90℃	Thermal	-
22	Three Bond	2105F + 2001	40000	180 at 100℃	Thermal	-
23	Three Bond	2247D	45000	30 at 150℃	Thermal	-
24	Fuller	EA 6411	50000	1 at 500mW	UV	Insoluble
25	Three Bond	2022 + 2105R	50000	60 at 100℃	Thermal	-
26	Three Bond	2086N	50000	30	Natural	-
27	Three Bond	2224C	64000	30 at 120℃	Thermal	-
28	Fuller	FH8708T	68260		UV	
29	Fuller	EM9002N	Unknown	1 at 90℃	Thermal	-
30	Henkel	Loctite Marine Epoxy	Unknown	120	Natural	Insoluble

Table 1. Adhesion candidates list for EHD

3.4.2. Adhesion applying using micro stage

Only using EHD, it is difficult to get high adhesive strength, so the limitation was supplemented through the process of adding an adhesive *EA6411* manufactured by *H.B.Fuller* with high cps 50,000 on top with a micro-tip on the micro-stage. By using the image processor of the vision-guided laser control system, the space between units is recognized, and the position information is transmitted to the micro stage program, and the adhesive is applied in such a way that the micro tip marks the joint position. The fabrication process is completed by removing the robot from the surface of glass treated with AF coating to lower the surface energy.

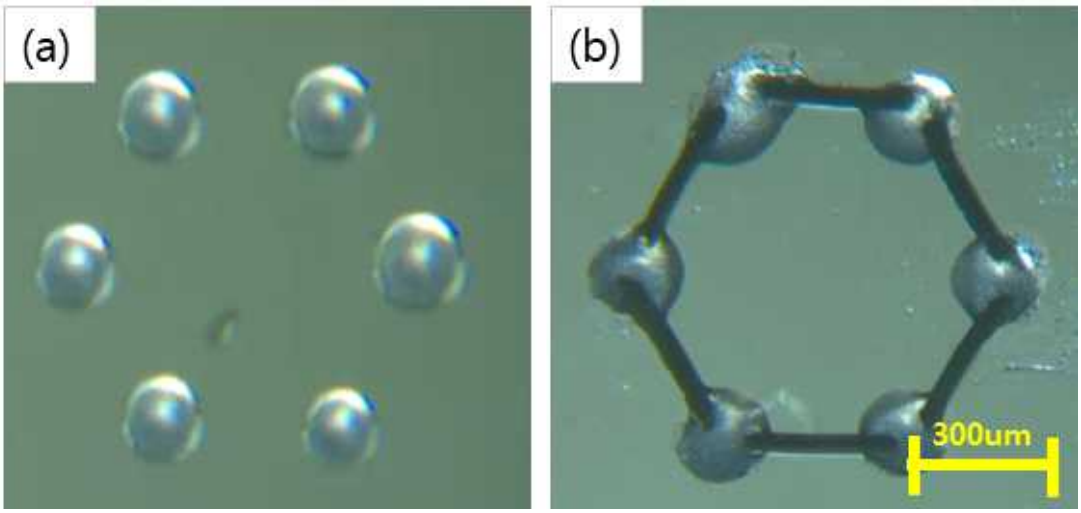

Figure 13. Adhesion applying with micro stage. a) adhesion applying test, b) the MTNs of the final completion up to adhesion applying with micro stage

Chapter 4. Experiment and Application

4.1. Force measurement experiments

We conducted the force measurement experiment to calculate the energy efficiency of the MTNs. Fig 14-b. shows the experiment setup prepared by attaching the MTNs to the *FT-S Microforce Sensing Probe* by *FemtoTools* that can measure up to 13.5 mN. Since the MTNs was stationary on the sensor tip, there was no drag force, and thus, we considered the measured force as purely a propulsion force. As a result of 10 times of experimentation, an average force of 7.7 mN was measured at a 40 mW/mm^2 laser.

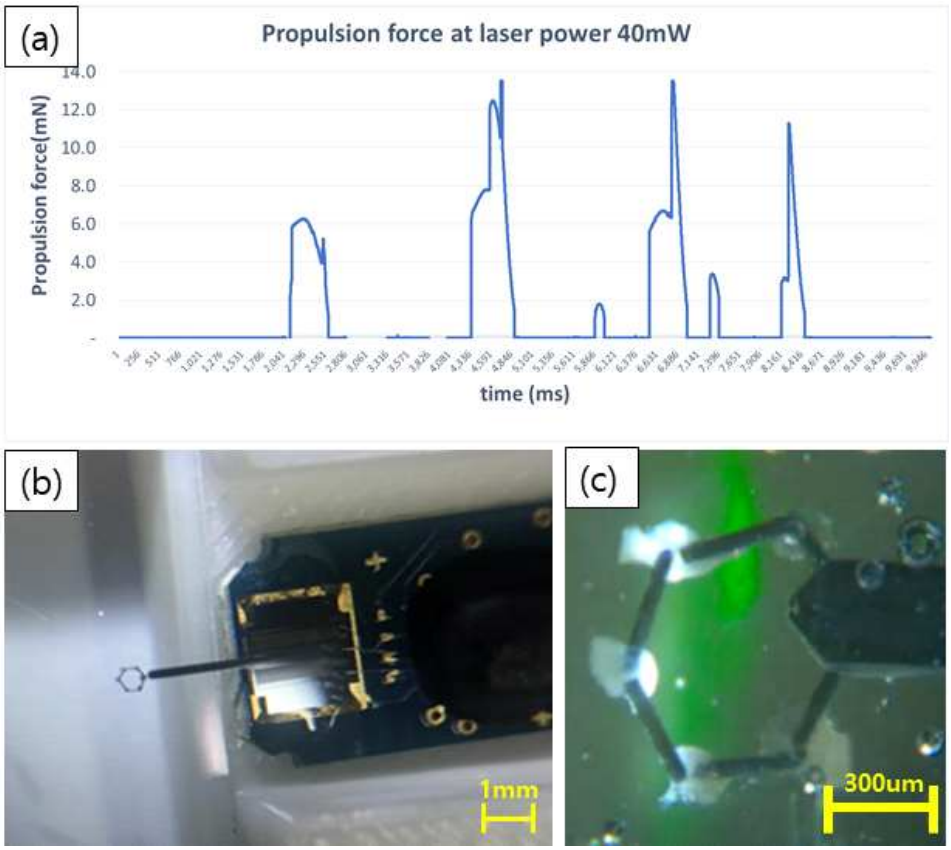

Figure 14. Propulsion force measurement experiment.
a) propulsion force graph of MTNs, b) force measurement experiment setup, c) capture of actual measurement experiment

4.2. Energy efficiency comparison

Based on the propulsion force and speed measurement of the MTNs, we calculated the power conversion efficiency of the micro robots and compared it with that of other light driven micro robots [8]. The efficiency is defined as Eq1.

$$\eta = P_{mechanical} / P_{light} \quad \text{.....(1)}$$

where $P_{mechanical}$ *is defined as*

$$P_{mechanical} = F_{propulsion} * v \quad \text{.....(2)}$$

Here $F_{propulsion}$ is the measured propulsion force and v is the speed. The efficiency, speed and type of light sources of representative light driven micro robots[8] and the MTNs are shown in Fig 5. The efficiency of the MTNs is estimated as $1.93 * 10^4$, whereas the efficiencies of other light driven micro robots are between the order of 10^5 and 10^{15}. As high power efficiency means that the micro robots require lower laser power to move, this can be the advantage in lower affection on the target or periphery region, which makes the MTNs more suitable for biomedical application.

Materials	Size [μm]	Mechanism	Supporting chemicals	Light intensity	Speed [μm s^{-1}]	Efficiency
Cu_2O@CDot sphere[155]	1.5 (D)	Self-electrophoresis	25 μM malic acid	≈150 mW cm^{-2} green light	40.85	7.5×10^{-9} a)
Pt/TiO_2 Janus sphere[176]	2.2 (D)	Self-electrophoresis	Pure water	40 mW cm^{-2} UV	8.9	9.6×10^{-10}
TiO_2–Au/Ag Janus sphere[177]	2 (D)	Self-electrophoresis	0.5 wt% H_2O_2	600 mW cm^{-2} UV	≈15	2×10^{-10} a)
p–n silicon nanowire[156]	0.5 (D) ≈10 (L)	Self-electrophoresis	70 μM ferrocenemethanol	≈70 mW cm^{-2} visible-light	≈500	2.3×10^{-6}
Cu_2O@N-CNT sphere[154]	1.5 (D)	Self-electrophoresis	30 mM glucose	≈150 mW cm^{-2} green light	18.7	1.6×10^{-9} a)
Sb_2Se_3/ZnO nanowire[56]	1 (D) ≈20 (L)	Self-electrophoresis	(10 mM/20 mM) BQ/H_2Q	≈600 mW cm^{-2} visible-light	≈15	4.3×10^{-11}
BiOI/metal Janus sphere[63]	2 (D)	Self-electrophoresis	Pure water	≈220 mW cm^{-2} green light	≈1.62	1.1×10^{-11}
CdS/C_{60} tube[178]	5 (D) 10 (L)	Bubble propulsion	5 wt% H_2O_2	UV-green	1058 ± 72	3.6×10^{-6} a)
TiO_2 tubular microengine[179]	6 (D) ≈90 (L)	Bubble propulsion	15 wt% H_2O_2	1 mW cm^{-2} UV	264	1.4×10^{-8} a)
Twin-jet-engine-microsystem[68]	≈800 (L)	Bubble propulsion	10% H_2O_2	Radiowave	1100	–
Cu/SiO_2 Janus particles[69]	6 (D)	Bubble propulsion	Water/glycerol	X-ray	1	8.7×10^{-13} a)
Carbonaceous nanobottle[180]	0.5 (D)	Thermophoresis	Not needed	0.74 W cm^{-2}	≈21	1.3×10^{-9}
$(PSS/PAH)_{20}$Au rocket[181]	5 (D) 50 (L)	Thermophoresis	Not needed	2×10^6 W cm^{-2} NIR	160	3.7×10^{-15}
PS/Au Janus sphere[182]	2 (D)	Opto-thermoelectric	0.2 mM CTAC	4×10^3 W cm^{-2}	15	3.4×10^{-14}

a)The presented efficiencies are estimated from the mechanical energy and incident light energy, without considering the energy from consumed chemicals. The mechanical energy calculation is adapted from previously reported method.[158] D: diameter; L: length.

Table 2. Energy efficiency table of light-driven micro robots[8]

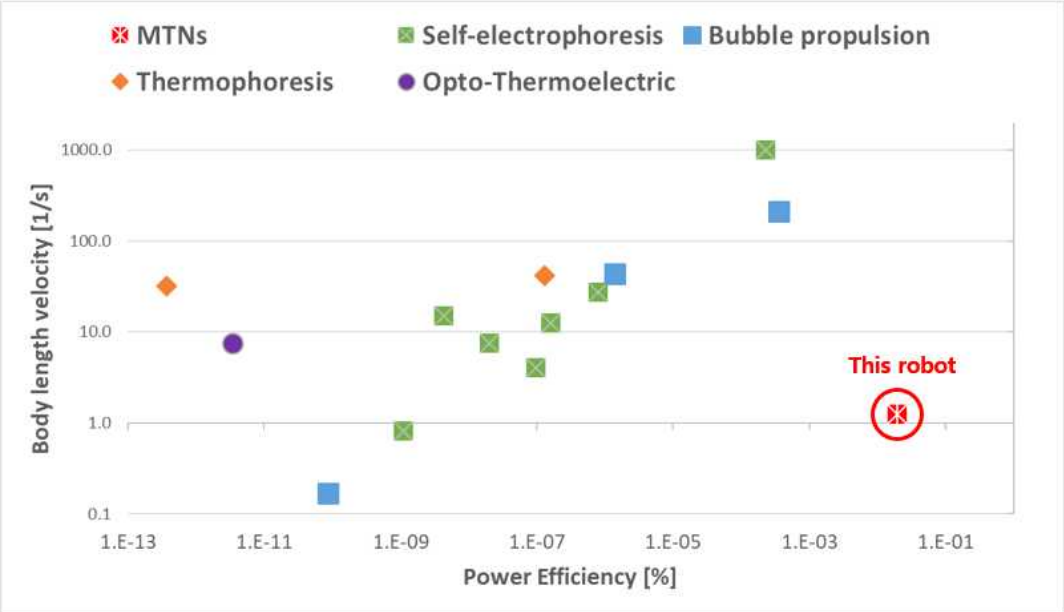

Figure 15. Energy efficiency comparison graph of light-driven micro robots

4.3. Functionality of transportation

The transport experiment was conducted to verify the transportation functionality of MTNs. A copper bead of 150 μm diameter and 130 μg mass was used as a target object due to its density being higher than water' s. The task of transporting a copper bead at 100 $\mu m/s$ over a 1,000 μg distance is completed without object loss. The MTNs is expected to transport multiple objects and maneuver through obstacle filled terrain environments. MTNs outperforms the Ni-Ti unit in terms of controllability due to its holding function. In the case of the Ni-Ti unit, there is a hassle of adjusting the orientation and position before transport in order not to lose the object, whereas the MTNs can be easily controlled because there is no risk of object loss.

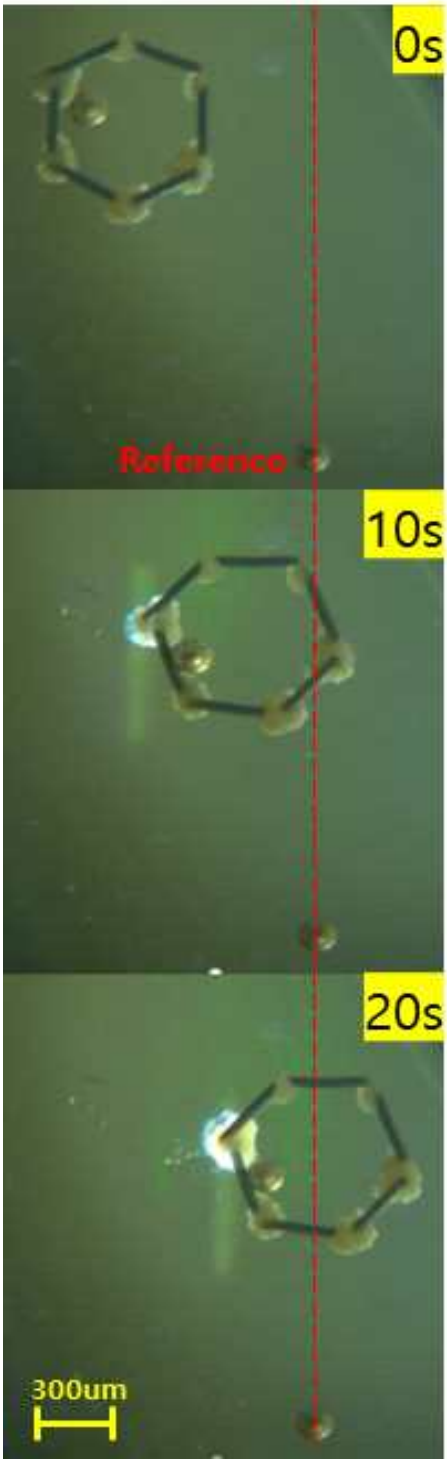

Figure 16. Demonstration of transport function of MTNs via copper bead transportation

Chapter 5. Conclusion

In summary, we have proposed a fine controllable Ni-Ti structure micro robot, which shows reliable transport capability. We designed the MTNs to be productive in terms of time, price and labor through fabrication process automation, commercial equipment and high yield materials. We succeeded in constructing a hexagonal shape structure by formation morphing control with the vision guided laser control system, bonding Ni Ti wire units using micro fluidic jet printer and confirming potential to deform the shape of robot according to objects and purposes. The relatively high energy efficiency of MTNs compared to other light-driven robots indicates that the MTNs operates with a low laser intensity which damage to surrounding area less, making it suitable for biomedical applications. The transportation experiment result demonstrates the stable transport functionality of MTNs with high controllability. The results of our work pave the way for a lab on a chip test that requires highly sophisticated transport using holding capability and controllability.

Our future work includes the integration of all processes into one system by attaching the bonding equipment to a vision guided laser control system instead of using EHD equipment. The current control system where only one robot at a time reacts to the laser to generate thrust also needs to be improved so that all robots can generate thrust simultaneously. We also aim to develop multi material robot that has several functions such as sensing, driving and holding.

Bibliography

[1] Jang, Ki-Hwan and Sung-Hoon Ahn. “Control of multiple Ni-Ti Units in High Speed using Laser” Dissertation, Seoul National University, 2020.

[2] Kim, Min-Soo, Hyun-Taek Lee, and Sung-Hoon Ahn. "Laser Controlled 65 Micrometer Long Microrobot Made of Ni-Ti Shape Memory Alloy." Advanced Materials Technologies, vol. 4, no. 12, pp. 1900583, 2019.

[3] Xie, Hui, et al. "Reconfigurable magnetic microrobot swarm: Multimode transformation, locomotion, and manipulation." Science Robotics, vol. 4, no. 28, 2019.

[4] Lee, Seungmin, et al. "A Capsule-Type Microrobot with Pick-and-Drop Motion for Targeted Drug and Cell Delivery." Advanced healthcare materials, vol. 7, no. 9, pp.1700985, 2018.

[5] Ta, Quang Minh, and Chien Chern Cheah. "Stochastic control for orientation and transportation of microscopic objects using multiple optically driven robotic fingertips." IEEE Transactions on Robotics, vol. 35, no. 4, pp. 861-872, 2019.

[6] A. Ichikawa, S. Sakuma, F. Arai, and S. Akagi. "Untethered micro-robot with gripping mechanism for on-chip cell surgery utilizing outer magnetic force." 2014 IEEE International Conference on Robotics and Automation (ICRA), pp. 3795-3800, 2014.

[7] Bae, Young K. "Photonic laser thruster: 100 times scaling-up and propulsion demonstration." Journal of Propulsion and Power vol. 37, no. 3, pp. 400-407 , 2021.

[8] Wang, Jizhuang, Ze Xiong, and Jinyao Tang. "The Encoding of Light-Driven Micro/Nanorobots: from Single to Swarming Systems." Advanced Intelligent Systems, vol. 3, no. 4, pp. 2000170, 2021.

[9] Bae, Young K. "Photonic laser propulsion: Proof-of-concept demonstration." Journal of Spacecraft and Rockets vol. 45, no. 1, pp. 153-155, 2008.

[10] Mahrle, Achim, and Eckhard Beyer. "Theoretical evaluation of radiation pressure magnitudes and effects in laser material processing." Physica Scripta, vol. 94, no.7, pp. 075004, 2019.

[11] Wang, Jizhuang, Ze Xiong, and Jinyao Tang. "The Encoding of Light-Driven Micro/Nanorobots: from Single to Swarming Systems." Advanced Intelligent Systems, vol. 3, no. 4, pp. 2000170, 2021.

[12] Adam, Georges, et al. "Stiffness Characterization and Micromanipulation for Biomedical Applications using the Vision-based Force-Sensing Magnetic Mobile Microrobot." 2020 International Conference on Manipulation, Automation and Robotics at Small Scales (MARSS), pp. 1-6, 2020.

[13] Hu, Wenqi, Kelly S. Ishii, and Aaron T. Ohta. "Micro-assembly using optically controlled bubble microrobots in saline solution." 2012 IEEE International Conference on Robotics and Automation. IEEE, pp.733-738, 2012.

[14] Jung, Youngho, et al. "Hybrid integration of III-V semiconductor lasers on silicon waveguides using optofluidic microbubble manipulation." Scientific reports

vol. 6, no. 1, pp. 1-7, 2016.

[15] Chen, Weinan, et al. "Magnetic/pH-sensitive double-layer microrobots for drug delivery and sustained release." Applied Materials Today, vol.19, pp. 100583, 2020.

[16] Fuchs, Katrin, et al. "Drug-eluting embolic microspheres for local drug delivery-State of the art." Journal of Controlled Release, vol. 262, pp. 127-138, 2017.

[17] Zhang, Dandan, et al. "Distributed Force Control for Microrobot Manipulation via Planar Multi-Spot Optical Tweezer." Advanced Optical Materials vol. 8, no. 21, pp. 2000543, 2020.

[18] Yao, Tianyi, et al. "Directed assembly and micro-manipulation of passive particles at fluid interfaces via capillarity using a magnetic micro-robot." Applied Physics Letters, vol. 116, no. 4, pp. 043702, 2020.

[19] Chen, Xiang-Zhong, et al. "Small-scale machines driven by external power sources." Advanced Materials, vol. 30, no. 15, pp. 1705061, 2018.

[20] Jiang, Wei, et al. "A dual-driven biomimetic microrobot based on optical and magnetic propulsion." Journal of Micromechanics and Microengineering, vol. 31, no. 3, pp. 035003, 2021.

[21] Martel, Sylvain, and Mahmood Mohammadi. "Using a swarm of self-propelled natural microrobots in the form of flagellated bacteria to perform complex micro-assembly tasks." 2010 IEEE International Conference on Robotics and Automation. IEEE, pp. 500-505, 2010.

[22] Li, Dengfeng, et al. "A fast and powerful swimming

microrobot with a serrated tail enhanced propulsion interface." Nanoscale, vol.10, no. 42, pp. 19673-19677, 2018.

[23] Grexa, Istv□n, et al. "Single-Cell Elasticity Measurement with an Optically Actuated Microrobot." Micromachines, vol. 11, no. 9, pp. 882, 2020.

[24] Mohanraj, Bhavana, et al. "Mechanically Activated Microcapsules for "On-Demand" Drug Delivery in Dynamically Loaded Musculoskeletal Tissues." Advanced functional materials, vol. 29, no. 15, pp. 1807909, 2019.

[26] Sun, Mengmeng, et al. "Cooperative recyclable magnetic microsubmarines for oil and microplastics removal from water." Applied Materials Today, vol. 20, pp. 100682, 2020.

[27] H. W. Kuhn, "The Hungarian method for the assignment problem". Naval Rcs. Loyisr. Q. , vol. 2, pp. 83-97, 1955.

[28] Li, Jinxing, et al. "Enteric micromotor can selectively position and spontaneously propel in the gastrointestinal tract." ACS nano, vol. 10, no. 10, pp. 9536-9542, 2016.

[29] Chatzipirpiridis, George, et al. "Electroforming of implantable tubular magnetic microrobots for wireless ophthalmologic applications." Advanced healthcare materials, vol. 4, no. 2, pp. 209-214, 2015.

[30] Li, Jinxing, et al. "Micro/nanorobots for biomedicine: Delivery, surgery, sensing, and detoxification." Science Robotics, vol. 2, no. 4, 2017.

[31] Hosseinidoust, Zeinab, et al. "Bioengineered and biohybrid bacteria-based systems for drug delivery." Advanced

drug delivery reviews, vol. 106, pp. 27-44, 2016.
[32] Dreyfus, Remi, et al. "Microscopic artificial swimmers." Nature, vol. 437, no. 7060, pp. 862-865, 2005.
[33] Ahmed, Daniel, et al. "Artificial swimmers propelled by acoustically activated flagella." Nano letters, vol. 16, no. 8, pp. 4968-4974, 2016.

초 록

마이크로 로봇은 원격 제어를 통해 시스템 내에서 미세작업을 수행할 수 있는 도구로써, 약물 수송, 수술, 진단과 같은 생물 의학 분야에서 많은 연구가 진행되고 있다. 마이크로 로봇은 외력을 통해 에너지를 공급받고, 제어되므로, 이용하는 외력의 종류에 따라 구동 특성이 달라진다. 여러 외력 중 광 구동형 마이크로 로봇은 정밀하고 국소적인 제어가 가능하다는 장점을 가지고 있다. 그러므로 정교한 제어가 필요한 마이크로 물체 운반 작업에 광구동형 마이크로 로봇이 적합하다. 지금까지 운송용 마이크로 로봇은 힘, 속도 및 제어에 중점을 두었지만, 물체 유실을 방지하기 위해 물체를 잡는 기능을 가진 로봇은 거의 없습니다. 우리가 개발한 미세 물체 수송 Ni-Ti 마이크로 로봇은 충분한 추진력과 속도를 가질 뿐만 아니라 운반 목표 물체를 포획한 상태로 외부 시스템과 격리한 상태로 운반할 수 있는 능력을 갖추고 있어 우수한 수송 안정성과 제어 편의성 등 이점을 보인다.

본 로봇은 비전 유도 레이저 제어 시스템에 의해 자동으로 제작이 가능하다. 양산을 고려하여 상용장비 만으로 제작 공정을 구성하였으며, 시간, 가격 그리고 노동력 측면에서 저렴하도록 마이크로 로봇을 설계하였다. 포획 능력과 향상된 제어 기능을 가진 본 로봇은 랩 온어 칩 테스트에서 액추에이터로 사용될 수 있다.

주요어 : 마이크로로봇, 레이저를 이용한 구동, 포메이션 모핑 제어
학 번 : 2019-24859